UNIVERSITY OF SOUTHERN CALIFORNIA

GEOPHYSICAL LABORATORY

TECHNICAL REPORT NUMBER 77-9

A Surface Wave Study of the South-China Subplate

Title of Contract:	Crustal and Upper Mantle Velocity and Q Structures of Mainland China
Reported By:	Robert Rosenthal and Ta-liang Teng
Contractor:	University of Southern California
Principal Investigator:	Professor Ta-liang Teng 213-741-6124
Contract Number:	F46920-76-C-0010
Program Code:	TF10-7F10
Effective Date of Contract:	July 1, 1976
Contract Expiration Date:	September 30, 1977
Amount of Contract:	$54,403

Sponsored by

August, 1977

83 04 07 11 0

DTIC
SELECTE
APR 7 1983

A

CONTENTS

LIST OF ILLUSTRATIONS

LIST OF TABLES

ABSTRACT

New data from the Seismological Research Observatory
(SRO) is used in conjunction with a non-linear least
squares technique to invert surface wave group velocity
data for the shear velocity structure of the South-China
subplate. A multi-filter analysis was used to produce
group velocities for the fundamental mode Love and
Rayleigh wave. A number of earthquakes over a single path
are used in order to deduce a measure of the observational
uncertainty of the present method. Group velocity standard
deviations range from .03 km/sec to .15 km/sec for Rayleigh
waves and .03 to .1 km/sec for Love waves over the period
range of 10 to 65 seconds.

Results of the inversion indicate that a 3 layer,
40 km thick crust is an adequate model consistent with the
data for the South-China subplate. Crustal shear veloci-
ties are found to be higher and upper mantle shear veloci-
ties lower than previously reported values for this
region.

Acknowledgments

This work is supported under ARPA Order No. 3291,
monitored by AFOSR under Contract No. F49620-76-C-0010.
Shelton Alexander and William Rodi have provided valuable
assistance and suggestions on methods of generalized
surface wave inversion.

INTRODUCTION

The China mainland consists of a number of tectonic subplates, each of geologically and geophysically distinct structures. Based on an investigation of the surface geology, Sun and Teng (1977) divide China into 4 basic tectonic units (Figure 1): (1) the Ching-Tibet subplate, (2) the North-China subplate, (3) the Northwest-China subplate, and (4) the South-China subplate. The present study focuses its attention on the South-China subplate. Specifically it makes use of a group of closely spaced earthquakes which give a number of pure-path surface wave trains recorded at a single SRO station. The resulting dispersion curves give a measure of the observational uncertainty of the surface wave data.

Using a non-linear least squares procedure based on the stochastic model (Franklin, 1970, Jordan and Franklin, 1970, and Derr et al., 1970), intermediate- and long-period group velocity data were inverted to obtain a detailed shear velocity model for the crustal and upper mantle structure of the South-China subplate (SOCHSP). Recently a number of large earthquakes and aftershocks have occurred at the boundary between the Ching-Tibet subplate and the South-China subplate. These events have been recorded at an SRO station at Taipei, Taiwan with

1
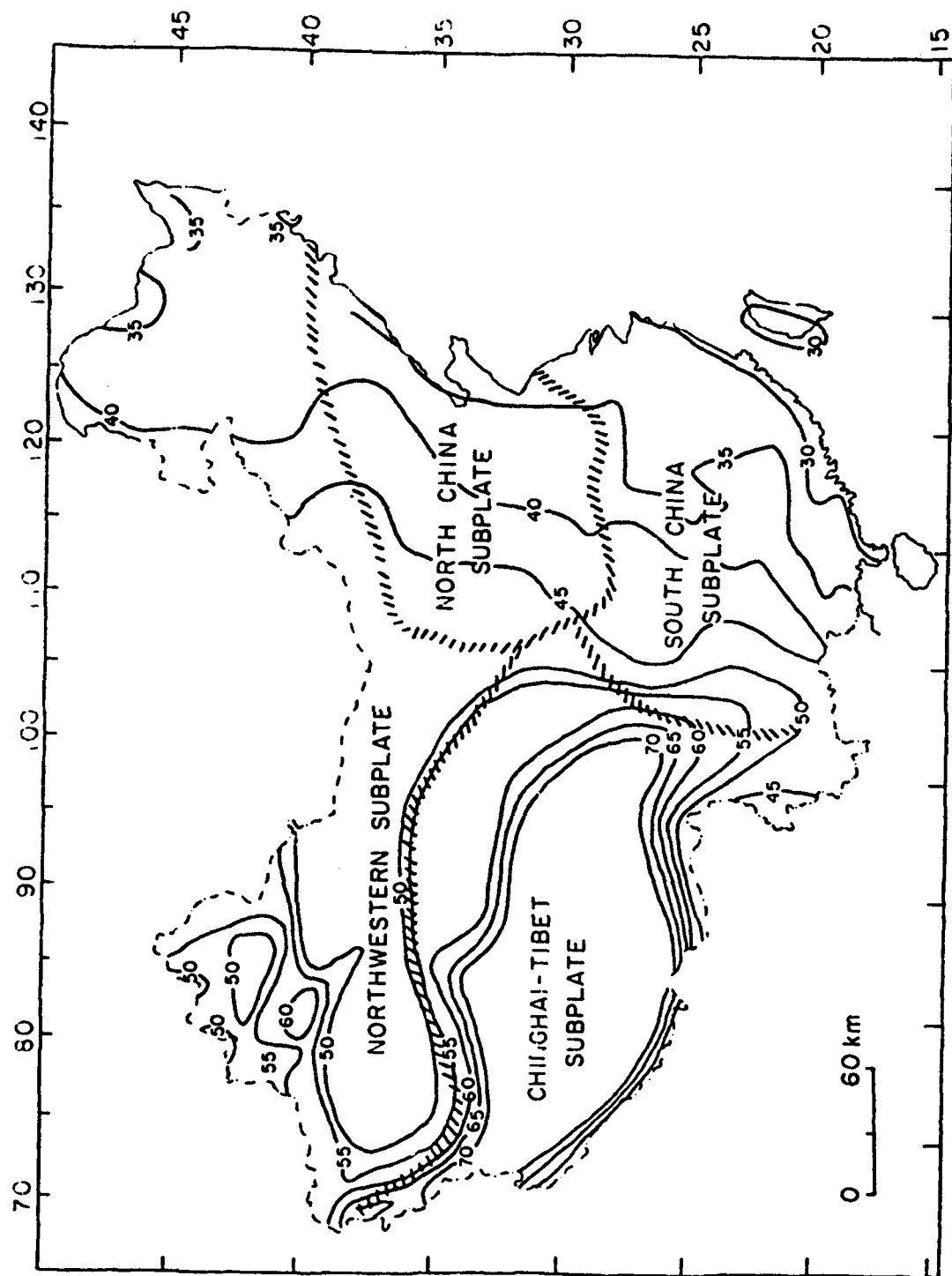
FIGURE 1. TECTONIC SUBPLATES OF CHINA

the station code TATO. SOCHSP is ideally suited for a surface wave study for three reasons: (1) the South-China subplate can be considered nearly laterally homogeneous (Tung, 1974; Sun and Teng, 1977); epicentral distances are adequate to allow an intermediate to long period dispersive wave train to develop; (3) seismic events occur and are recorded within the subplate, thus eliminating the effects of crossing plate boundaries.

Lacking good geophysical data, most of the previous seismological studies were either limited to a simple estimate on the crustal thicknesses and shallow crustal structures or lacked a discussion of model resolution and standard deviation. Knowledge about the crustal and mantle shear velocity structure of SOCHSP is poor. Tseng and Sung (1963) determined crustal thickness by applying the tripartite method (Press, 1956) to two events from the New Britain Islands for phase velocity information. The inversion results of their study are seen in Figure 2. The numbers inside each triangle represent the average crustal thickness within three stations. Using short period (4-12 seconds) Rayleigh and Love wave group velocity dispersion, Sung et al. (1965) determined the thickness of the sedimentary layers for several regions in China. Tung (1974) made use of long period group velocity data and tried to obtain a shear velocity structure for SOCHSP. But the method he used was

3

FIGURE 2

FIGURE 2
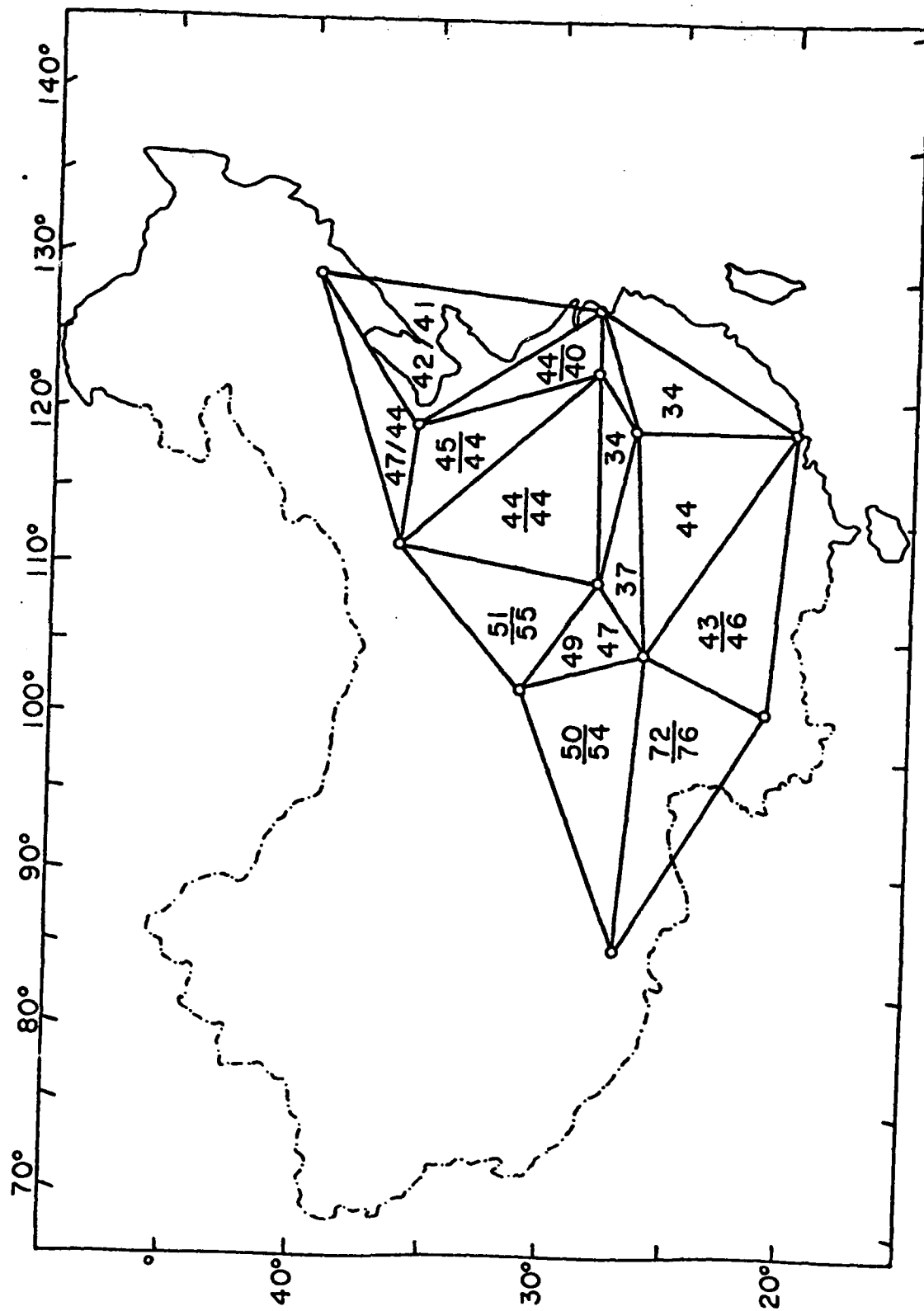
essentially a trial-and-error surface wave inversion technique and thus he was unable to give a discussion about resolution or standard deviation of his resulting models.

Previous work has illustrated that Rayleigh waves produce more information about earth models than Love waves (Wiggin, 1972; Derr and Landisman, 1972). Wiggins (1972) has shown that by simultaneously inverting Love and Rayleigh wave data, it is possible to obtain both shear wave and density structures. Though group velocity and phase velocity contribute almost the same information (Bloch, 1969, Bloch et al., 1969, Wiggins, 1972), Bloch (1969) and Fix (1975) come to the conclusion that group velocity is more sensitive to the earth model and therefore should produce better resolution in the inversion. Through a multiple filtering technique, this study first obtains group velocity measurements from the fundamental mode Love and Rayleigh waves, followed by a Gilbert-Backus (1967, 1968) type inversion to obtain a crustal and upper mantle structure of SOCHSP together with an estimate of model standard deviation and resolution.

SOUTH-CHINA SUBPLATE

The South-China subplate (SCS) is bounded on the south and east by the Pacific Ocean, on the west by longitude 103°E, and on the north by latitude 32°N (Figure 3). From previous gravity and seismic studies (Tseng and Sun, 1963; Tseng, 1973; Tung, 1974) the crustal thickness of SCS is believed to increase from 30 km at the eastern boundary to 50 km at the western boundary with an average thickness of 40 km.

The subplate is composed of two parts, the Yangtze fault block in the northwest and the South-China folding block in the southeast. The Yangtze fault block is a section of old continental crust formed during the Jinning Orogeny (1300-950 m.y.), and was subsequently faulted and strongly metamorphosed. Formed during the Caledonian Orogeny (570-400 m.y.), the South-China folding block was a section of transitional (miogeosynclinal) crust that later underwent weak metamorphism and folding. (Tectonic Map Compiling Group, 1974, Guizhou Geologic Team 103, 1975).

While surrounded by a number of seismically active zones, SOCHSP is one of the most stable regions in China. Though a number of large events occur on or beyond its western boundary, which marks the India-Eurasia collision,
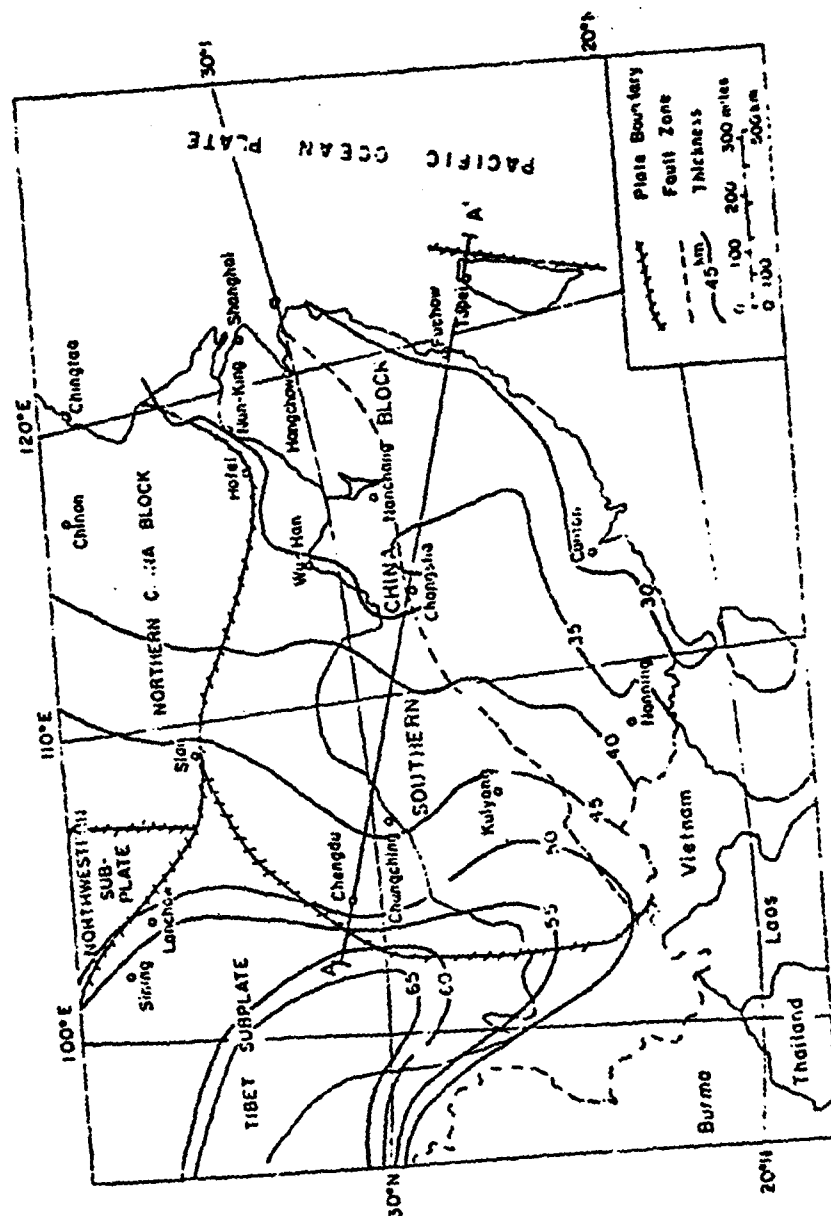
FIGURE 3. THE SOUTH-CHINA SUBPLATE

there are only a few interplate earthquakes (Figure 4).
According to Li et al. (1974), this can be explained by
the fact that this region has undergone weaker metamorphism
than other regions and therefore, the rocks are softer and
do not lend themselves to high stress accumulation.

DATA

The data used in this study are surface waves from
four earthquakes (Table 1) focused in the Szechwan
Province of mainland China. The events were recorded at
SRO station TATO. A number of events over one path were
desired in order to establish data repeatability and to
obtain observational uncertainties. Because of instrument
problems and poor dispersion results (due to the arrival
of wave energy at certain periods that have taken non-
least-time paths), certain components of individual
earthquakes were not used in obtaining group velocity
information. The epicentral region and path are shown
in Figure 3 (4-4').

SRO data in digital form on tape is convenient for
computer processing techniques and the storage of a large
amount of information on a single data tape. The SRO
station operates at high sensitivity thus expanding the
detection threshold for seismic events making small
magnitude events ($M \sim 5$) useful for surface wave analyses.
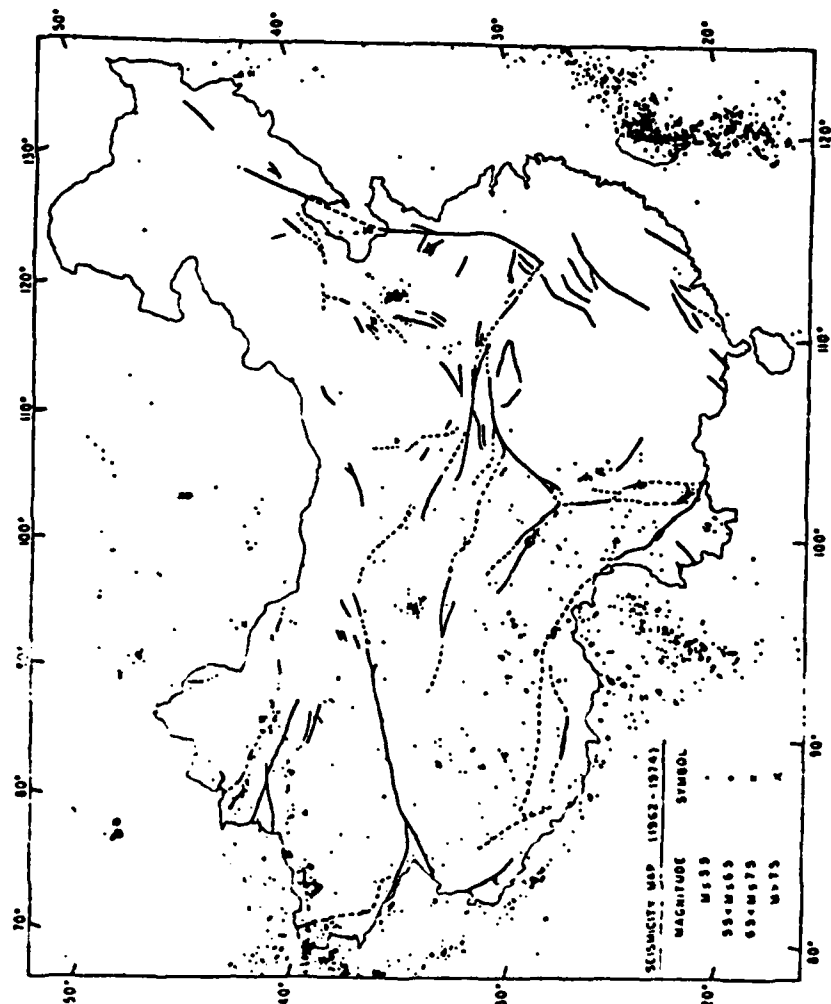
Map showing distribution of epicenters of recent earthquakes in China (1962–1974) using Albers equal-area projection.

FIGURE 4

9

TABLE 1

LIST OF SEISMIC EVENTS

Date	Location	Focal Depth (km)	Magnitude	Epicentral Distance (km)
August 19, 1976	32.893N 104.189E	33	5.4	1902.0
August 22, 1976	32.992N 104.181E	33	4.7	1884.0
September 1, 1976	32.460N 104.152E	18	5.1	1886.0
September 3, 1976	28.040N 100.345E	33	5.2	1854.0

With this new system, the amount of data available for long-period surface waves studies is greatly increased.

SRO datatapes contain data from three long-period channels, sampled at the rate of once per second and one vertical component sampled at the rate of twenty times per second. Long-period data is recorded continuously on tape; short-period data is recorded only when an event has been detected, and is sampled at the rate of twenty times a second. The vertical, north-south, and east-west long period channels are multiplexed into each record. Each SRO data record consists of 1000 words (2000 bytes). The first ten words are header information. The next 990 words are data; therefore, there are 5 minutes, 30 seconds of data per long period record (Peterson et al., 1976).

The amplitude and phase response for the long-period instrument is given in Table 2. An analytic form of the transfer function used in our computer program is found by numerically fitting the amplitude and phase response into a polynomial. The transfer function has the form:

$$\frac{\sum_{i}^{n} a_i z^i}{\sum_{i}^{n} b_i z^i}$$

where: $a_0 = 1.7443 \times 10^{-4}$ $a_1 = 3.1635 \times 10^{-3}$

         $a_2 = .21163$ $a_3 = .14127$

TABLE 2

Frequency	Relative Amplitude	Phase Angle (Radians)
.0667	.460	-1.33
.05556	.672	-1.00
.04546	.912	-0.63
.04	1.00	-0.42
.0333	1.01	-0.13
.02778	.9	0.10
.02326	.724	0.30
.02	.550	0.47
.01667	.400	0.63
.0125	.200	0.92
.01	.108	1.10
.00667	.031	1.34
.005	.0104	1.51
.0025	.00084	1.84
.00167	.000184	2.00

$$b_0 = 3.531 \times 10^- \qquad b_1 = 3.3316 \times 10^{-2}$$

$$b_2 = .12378 \qquad b_3 = 1.0$$

A plot of this transfer function is given in Figure 5.

Each seismic event must be decoded and plotted from the data tapes. Pure Love waves are obtained by rotating the data coordinates. An example of a plotted seismic event before and after coordinate rotation is given in Figure 6 and 7.

A multiple filtering analysis (Dziewonski and Hales, 1970; Hermann, 1973; Tung, 1974; Seekins and Teng, 1976) has been applied to the surface wave train to obtain group velocity dispersion curves. A typical contoured result of this type of analysis is shown in Figure 8. Because of the epicentral distances involved, only periods of up to 65 seconds were used for Rayleigh waves and 50 seconds for Love waves. The dispersion curves for the fundamental mode Love and Rayleigh waves are plotted in Figures 9 and 10. In these figures, the solid line represents the average group velocities obtained from the multiple filtering analysis. The statistical properties of the observations are listed in Table 3 and 4.

THEORY

Generalized least squares methods for determining the Earth's structure from seismic data have been formulated by

PHASE in DEGREES

SRO TRANSFER FUNCTION

□ SRO Phase
○ SRO Complex Gain

FREQUENCY

FIGURE 5

GAIN in DB

14

N-S
COMP.

VERTICAL
COMP.

E-W
COMP.

SECONDS
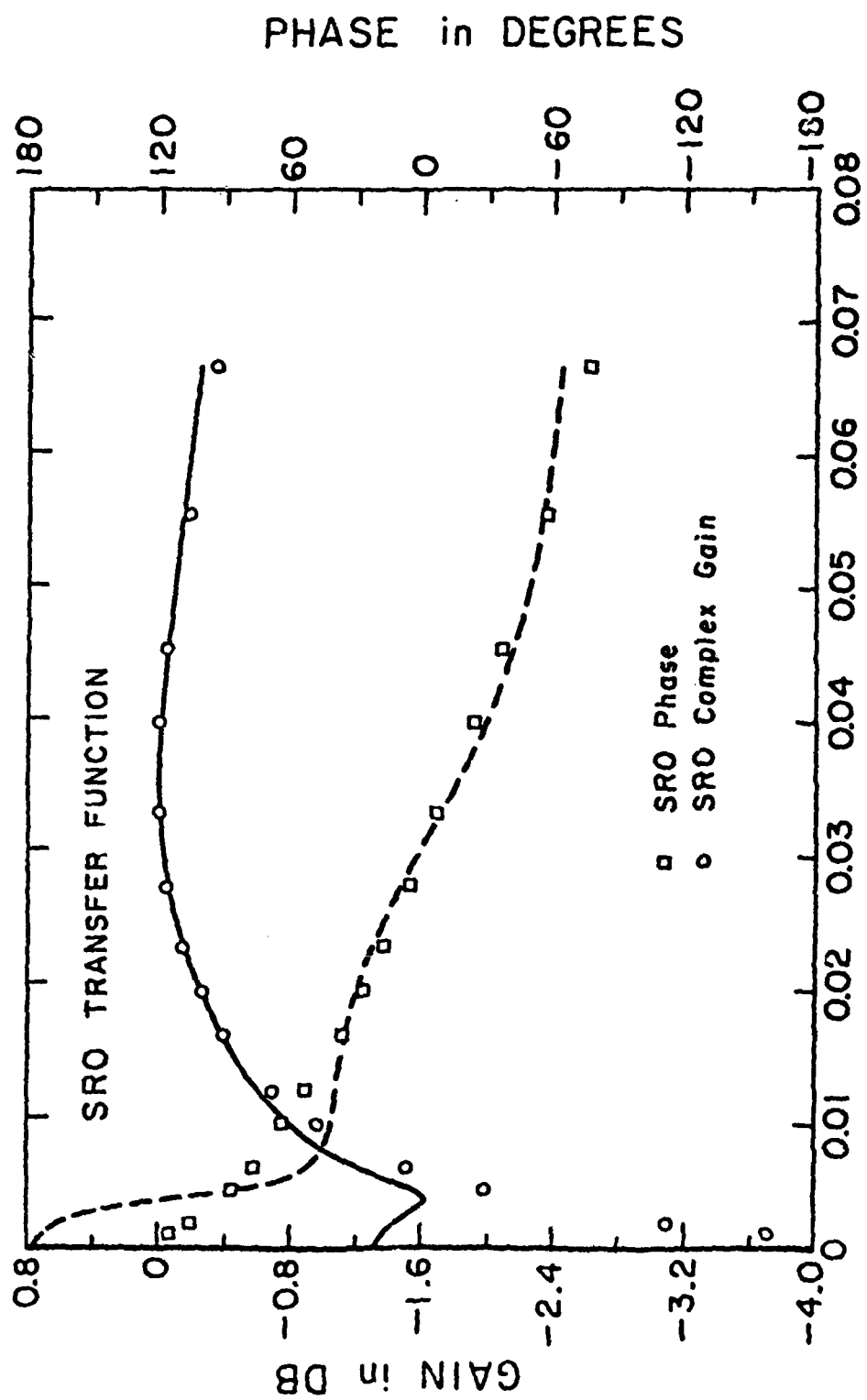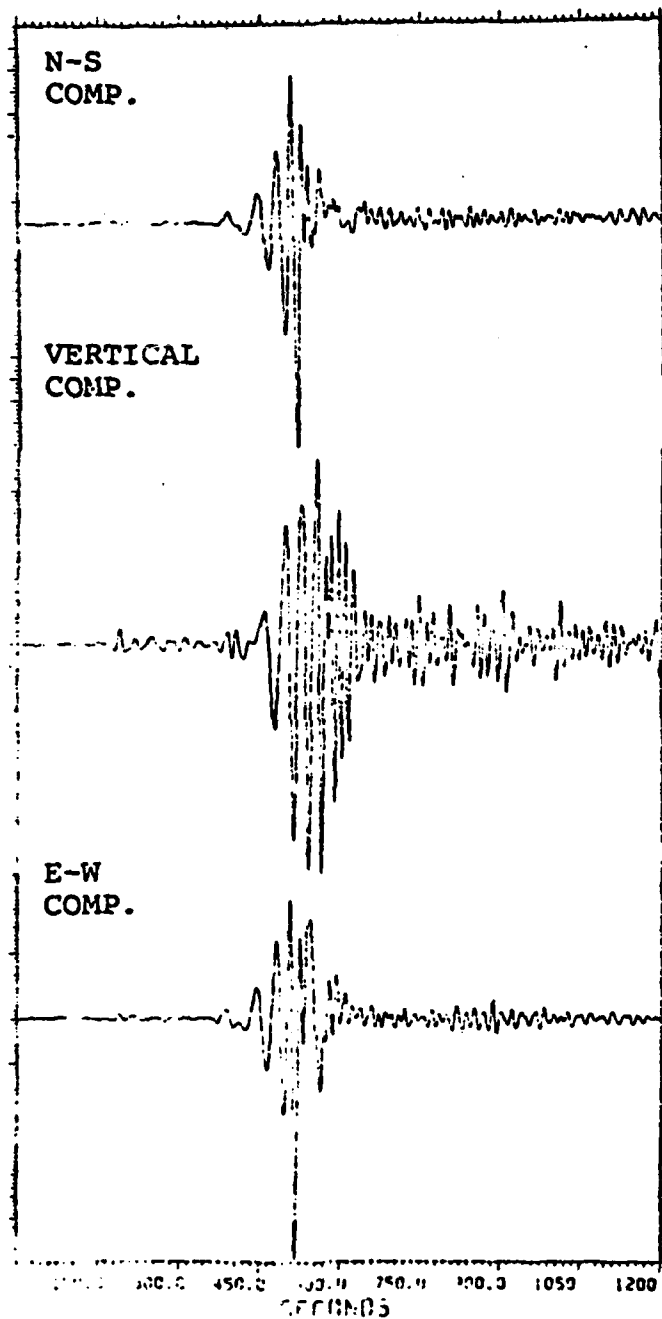
FIGURE 6

UNROTATED SEISMOGRAM   8/18/76

15
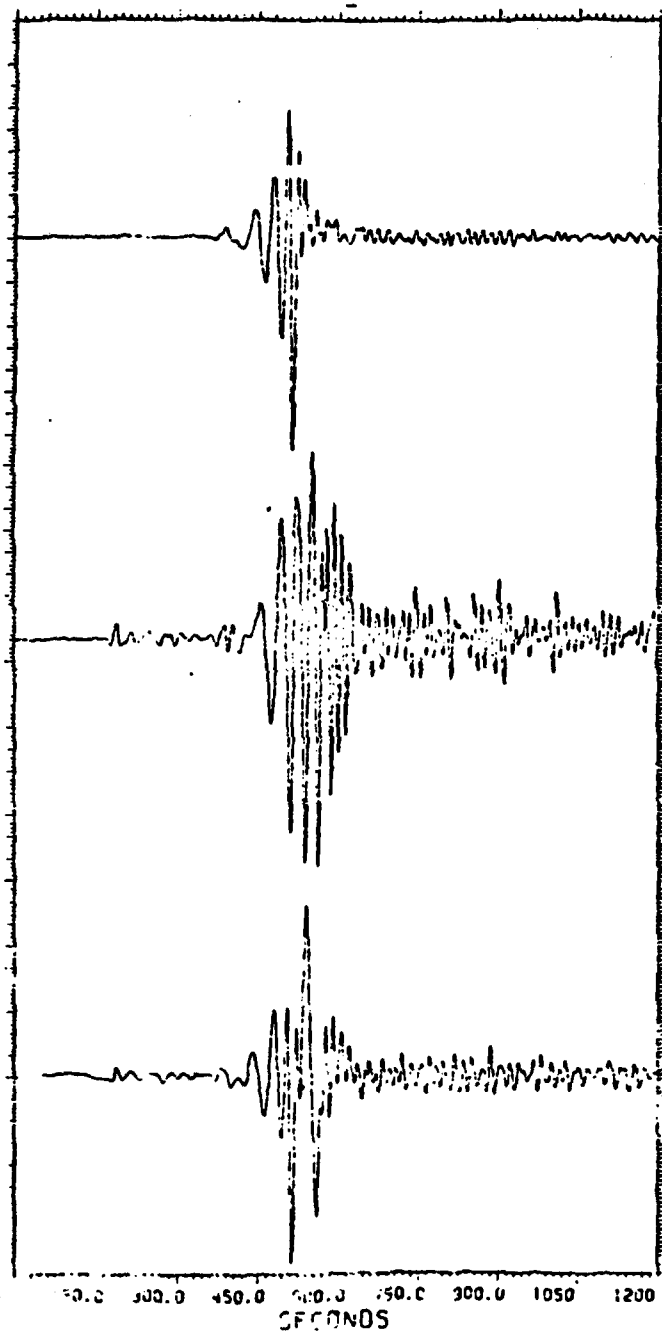
FIGURE 7

ROTATED SEISMOGRAM   8/18/76
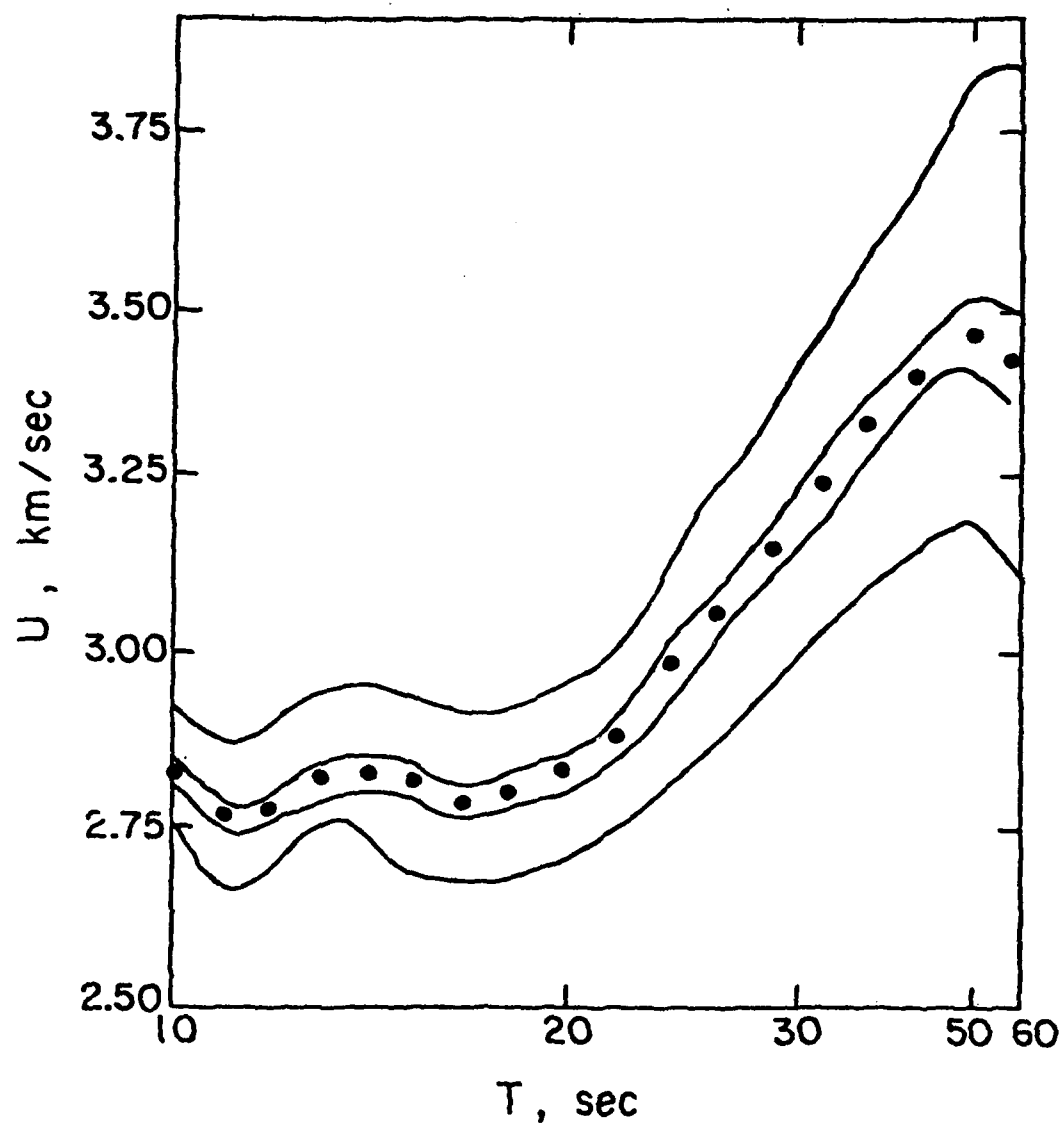
FIGURE 8

MULTI-FILTER ANALYSIS OF VERTICAL COMPONENT

9/1/76

17

FIGURE 9

18

LOVE WAVE

Averaged Observed Data
● 9/1
▽ 9/3

T , sec

U , km/sec

FIGURE 10

19
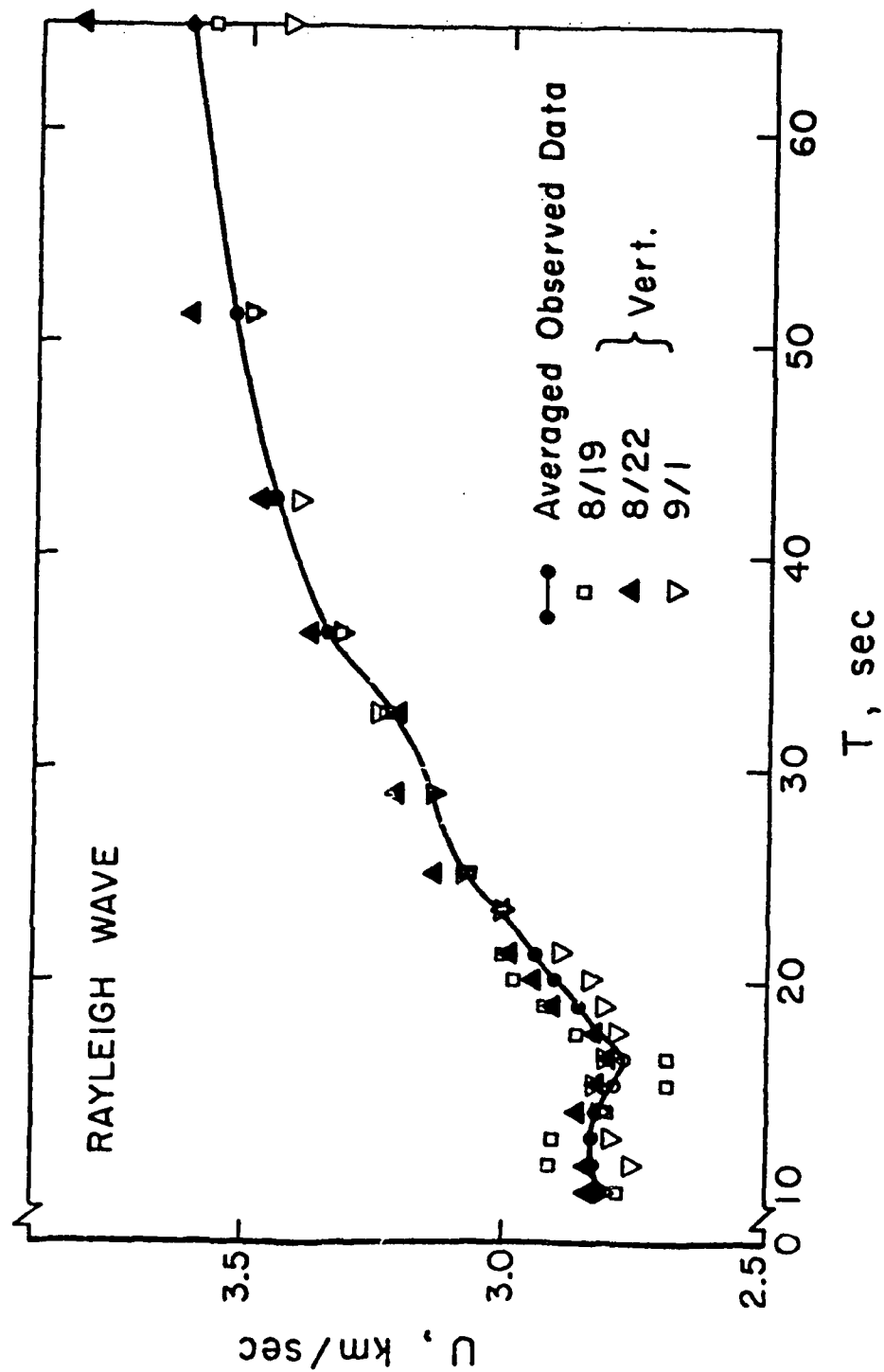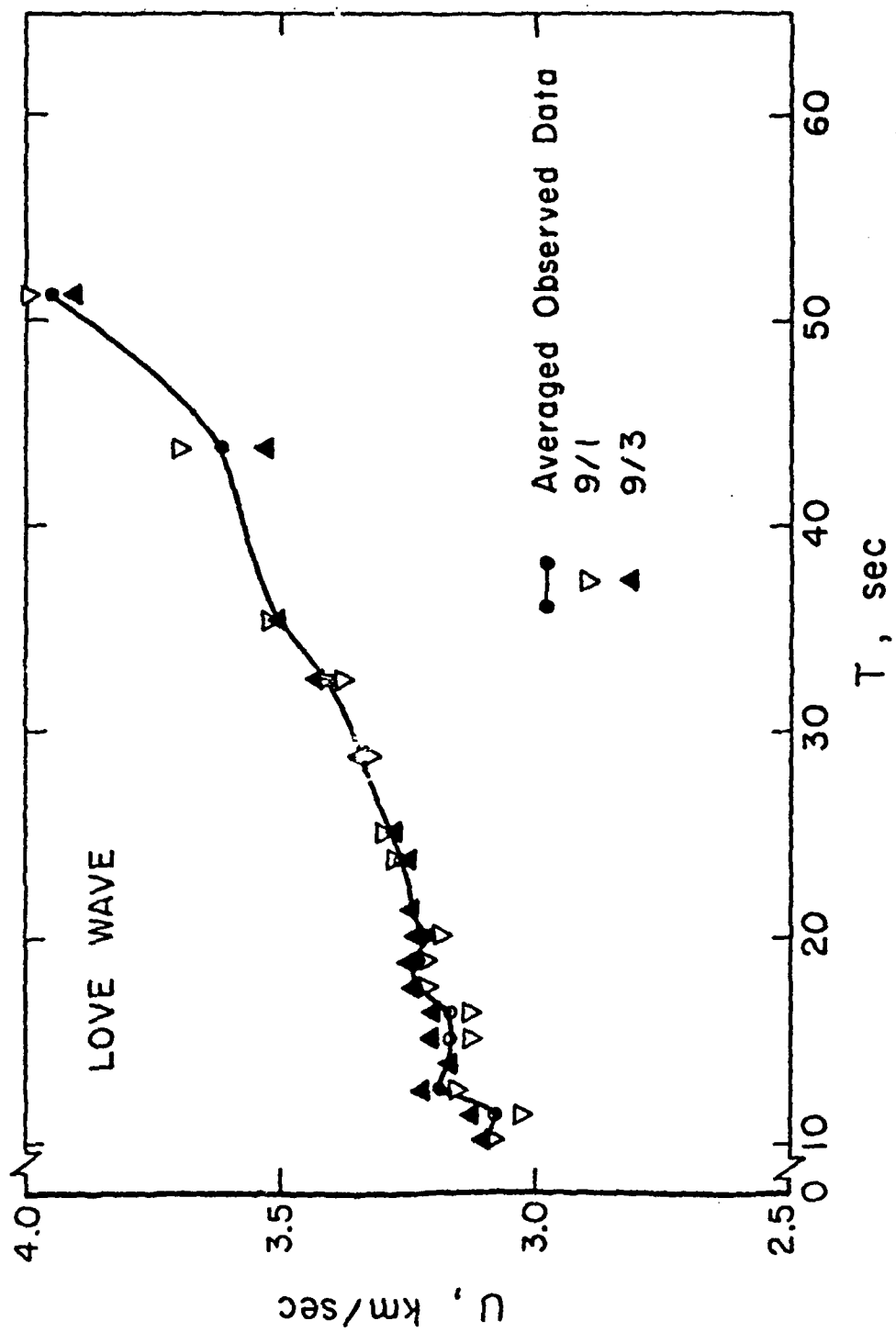
TABLE 3

RAYLEIGH WAVE

PERIOD	AVERAGED OBSERVED GROUP VELOCITY (KM/SEC)	ESTIMATED STANDARD DEVIATION
64.00	3.61	.15
51.20	3.54	.07
42.667	3.44	.04
36.571	3.35	.03
32.00	3.23	.03
28.444	3.14	.03
25.60	3.07	.03
21.333	2.95	.06
19.692	2.91	.06
13.236	2.86	.05
17.067	2.83	.05
16.00	2.77	.07
15.059	2.78	.07
13.474	2.83	.03
12.19	2.83	.06
11.13	2.83	.06
10.24	2.81	.03

TABLE 4

LOVE WAVE

PERIOD	AVERAGED OBSERVED GROUP VELOCITY (KM/SEC)	STANDARD DEVIATION
51.2	3.95	0.1
42.667	3.61	0.1
36.571	3.52	.03
32.00	3.41	.03
28.444	3.35	.03
25.60	3.29	.03
23.273	3.26	.03
21.333	3.24	.03
19.692	3.22	.03
18.286	3.24	.03
17.067	3.23	.03
16.00	3.17	.04
15.059	3.17	.05
13.474	3.17	.03
12.19	3.19	.04
11.13	3.08	.06
10.24	3.09	.03

numerous authors (Jackson, 1972; Wiggins, 1972; and Crosson, 1976). The basic logic in the inversion theory is as follows:

The observations, Y_i, are related to certain model parameters, X_j, in some known way, $Y_i = A(X_1, X_2, \ldots X_p)$. A quasi-linear relationship is established by taking a Taylor series expansion about some initial value X_0'.

$$Y_i = A_i(X_0') + \frac{\partial A_i}{\partial X_j} \Big|_{X_0'} \Delta X + \text{higher order terms}$$

$$Y_i \equiv A_i(X_0') + \Delta Y_i$$

Ignoring the higher order terms, we obtain the functional relationship:

$$\Delta Y_i = \frac{\partial A_i}{\partial X_j} \Big|_{X_0'} \Delta X_j \qquad (1)$$

where ΔY_i = observed data minus calculated observations. Equation 1 in matrix form becomes:

$$A\Delta X = \Delta Y$$

Where A is a matrix whose elements are the partial derivatives in Equation 1, ΔX is a p x 1 vector whose elements are correction to the initial model vector X_0', and ΔY is the difference between the observed and theoretical data.

In our case the observations are group velocities of

Love and Rayleigh waves, and the model parameters are shear velocities and densities for a horizontally layered earth. The partial derivatives in equation 1 are generated numerically by the method described by Rodi et al. (1975).

The classic least squares solution to equation 2 is by minimizing the euclidean length of $A\Delta X - \Delta Y$ or

$$\| A\Delta X - \Delta Y \| = (A\Delta X - \Delta Y)^{T}(A\Delta X - \Delta Y) = \epsilon$$

Given equation 2, the solution is (Hanson and Lawson, 1975):

$$A\Delta X = \Delta Y$$
$$A^{T}A\Delta X = A^{T}\Delta Y$$
$$\hat{\Delta X} = (A^{T}A)^{-1}A^{T}\Delta Y$$

where $\hat{\Delta X}$ is the estimated correction vector.

A suitable inverse to this problem can be obtained by using the singular value decomposition (SVD) of the matrix A.

$$A = U\Lambda V^{T}$$

where the columns of U are the eigenvectors associated with the colums of A, the rows of V are the eigenvectors associated with the rows of A, and Λ is a diagonal matrix of non-zero eigenvalues of the matrix A.

23

$$
\Lambda = A^T A = \begin{vmatrix} \lambda_1 & \cdot & \cdot & \cdot & \cdot \\ 0 & \lambda_2 & \cdot & \cdot & \cdot \\ \cdot & \cdot & \cdot & \cdot & \cdot \\ & & & & \\ 0 & \cdot & \cdot & \cdot & \lambda \end{vmatrix}
$$

If we let

$$
H = (A^T A)^{-1} A^T \tag{3a}
$$

then

$$
HA\Delta X = H\Delta Y \tag{3b}
$$

and

$$
\hat{\Delta X} = HA\ X \tag{3c}
$$

and

$$
\hat{\Delta X} = H\Delta Y
$$

Using the SVD we obtain (Jackson, 1972):

$$
\hat{\Delta X} = (\Lambda V^{-1} U^T)\Delta Y \tag{3d}
$$

$$
H = \Lambda V^{-1} U^T
$$

Here, H is known as the pseudo-inverse of equation 2.

The matrix product HA=R is known as the resolution matrix, and is a measure of the uniqueness of the solution (Jackson, 1972). The rows of R are called the resolving kernals. From equation 3c, it can be seen that an element of $\hat{\Delta X}$, $\hat{\Delta X}_i$, may be interpreted as convolving the ith row of R with the vector ΔX. Therefore, ΔX_i can be considered the weighted sum of nearby values (Jackson, 1972).

24

Because $A^T A$ is nearly singular, a number of problems arise: (1) The solution vector becomes large which can cause the problem to leave the region of linearity; (2) the solution oscillates with each iteration. By looking at the pseudo-inverse H we can see the cause of this instability.

$$H = V \Lambda^{-1} U^T$$

where the matrix Λ^{-1} equals

$$\Lambda^{-1} = \begin{vmatrix} \frac{1}{\lambda_1} & 0 & \cdot & \cdot & \cdot & \cdot \\ 0 & \frac{1}{\lambda_2} & 0 & \cdot & \cdot & \cdot \\ \cdot & \cdot & \cdot & \cdot & \cdot & \cdot \\ \cdot & \cdot & \cdot & \cdot & \cdot & \cdot \\ 0 & \cdot & \cdot & \cdot & \cdot & \frac{1}{\lambda_n} \end{vmatrix}$$

and the λ_i's are the eigenvalues of the matrix $A^T A$. If $A^T A$ is near singular, one or more of the eigenvalues will be approaching zero. From equation 3 it can be seen that a small eigenvalue will cause a large change in one or more values of the correction vector $\Delta \hat{X}$. Similarily, it has been shown that the variance of the model parameters are inversely proportional to λ (Jackson, 1972). Thus small λ's produce large standard deviations.

There are two main approaches to stabilizing the inversion process. One method is to examine the

eigenvalue spectrum of the matrix A. Small eigenvalues are removed when the variance becomes too large. But removing the eigenvalues degrades the resolution. This trade-off between resolution and variance has been discussed by a number of authors (Jackson, 1972; Wiggins, 1972; and Crosson, 1976). Braille and Keller (1975) used this method for the inversion of group velocity data.

Inversion stability can also be achieved by using Marquardt's method (Marquardt, 1963) or the stochastic inverse (Franklin, 1970). These procedures lead to the suppression of small eigenvalues. Franklin's stochastic inverse estimates the parameter in the presence of noise. Equation 2 becomes:

$$A\Delta X + n = \Delta Y \qquad (4)$$

there n is a vector of observational noise. Franklin (1970) shows that the solution to equation 4 is given by:

$$\Delta X = WA^T (AWA^T + ED)^{-1} \Delta Y \qquad (5)$$

where W is the covariance matrix of the parameter and ED is the covariance matrix of the observations.

Marquardt's method considers a minimization of the functional

$$(A\Delta X - \Delta Y)^T (ED^T ED)(A\Delta X - \Delta Y) - \Delta X^T (W^T W) \Delta X \qquad (6)$$

26

with the solution given by:

$$\Delta X = (A^T E D^{-1} A + W_p^{-1})^{-1} A^T E D^{-1} \Delta Y \qquad (7)$$

Letting $A^T E D^{-1} = A^T$, equation 7 becomes:

$$\Delta X = (A^T A + \sigma^2 I) A^T \Delta Y \qquad (8)$$

where σ^2 is the variance of the parameter.

By looking at the SVD of equation 8 we can see how Marquardt's method tapers the eigenvalue spectrum:

$$\Delta X = V |(\Lambda^2 + \sigma^2 I)^{-1} \Lambda| U^T \Delta Y \qquad (9)$$

An element in brackets from equation 9 equals: (Crosson, 1976)

$$|(\Lambda^2 + \sigma^2 I)^{-1} \Lambda|_i = \lambda_i / (\lambda^2{}_i + \sigma^2)$$

So as λ_i goes to 0, the parameter ΔX_i goes to zero. A similar analysis for the stochastic inverse shows that it too suppresses small eigenvalues.

The quantity σ^2 can also be thought of as a trade-off parameter between resolution and variance (Der et al., 1970; Wiggins, 1972; Crosson, 1976). In Marquardt's method, the resolution equals (Crosson, 1976):

$$R = HA = (A^T A + \sigma^2 I) A^T A = V |(\Lambda + \sigma^2 I)^{-1} \Lambda^2| V^T \qquad (10)$$

For the stochastic inverse

27

$$R = \left| (\Lambda^2 + \sigma^2 I)^{-1} \Lambda^2 \right| VV^T \qquad (11)$$

The quantity in brackets of equations 10 and 11 is a diagonal matrix whose elements have the form:

$$\lambda_i^2/(\lambda^2 + \sigma^2)$$

If $\sigma^2 = 0$, then $R = I$, but as σ^2 goes to 0 the variance of the parameters becomes larger. So we adjust the size of σ^2 until there is an acceptable trade-off between standard deviation and resolution.

Two other elements that must be analyzed in the inversion process are the apriori (SDX_0) and postpriori (SDX) standard deviations of the inversion parameters:

$$SDX_0 = D^T (\sigma W P^{-1}) D$$

$$SDX = \sqrt{D^T (A^T E D^{-1} A + \sigma W P^{-1})^{-1} D}$$

where D = a row vector of a delta matrix = $(0,0,\ldots,1,\ldots 0)$. This analysis will give a measure of how much new information is coming from the data. If SDX_0 and SDX are approximately the same, we know that very little information is coming from the data.

The advantages of Marquardt's method and the stochastic inverse is that the SVD of A is not explicitly determined and there is no decision to be made on the rank of the matrix $A^T A$.

A combination of these two methods are used in our

28

inversion process. When the number of parameters is greater than the number of data, the stochastic inverse is used. If the number of observations is greater than the number of parameters, Marquardt's method is used. This procedure leads to the minimum number of computations.

DISCUSSION

Initial models for the inversion were based on the results of a previous surface wave study done by Tung and Teng (1974). Their final model was obtained from Love and Rayleigh wave group velocity data. Our starting model (M1, Table 5) was inverted for both shear velocity and density.

During the inversion, large instabilities of the density parameter were found in the crust. This was corrected by changing the starting model and inverting for compressional wave velocity. In the derived model (DM1) a low velocity layer (LVL) can be inferred in the sixth layer, but the validity of this LVL is questionable because of the insufficient data in our study. Examination of the apriori and postpriori standard deviations for the shear velocity parameter (Table 5) shows that there is only a small amount of information in the data applicable to depths below the fifth layer. Thus longer period information is needed to confirm velocities beyond

29

TABLE 5

STARTING MODEL
M1

LAYER THICKNESS (KM)	D-VELOCITY (KM/SEC)	SHEAR VELOCITY (KM/SEC)	DENSITY
10	5.0	3.0	3.0
10	5.0	3.1	3.05
20	6.0	3.5	3.2
20	8.40	4.6	3.3
25	8,05	4.55	3.34
50	7.80	4.2	3.37
50	8.00	4.3	3.37

FINAL MODEL
DM1

SHEAR VELOCITY (KM/SEC)	SDX_0	SDX
3.245	.277	.046
3.193	.277	.076
3.767	.196	.055
4.498	.196	.106
4.495	.175	.112
4.283	.124	.105
4.435	.124	.120

this depth.

A new initial model (M2) using thinner layers in the crust and mantle was inverted for shear wave velocity, density and compressional wave velocity. The mantle shear velocities for M2 were also modified, as were density and P velocity values in the crust (Table 6).

By examining the relative sizes of the partial derivatives of different parameters, we can determine the importance of each parameter in the inversion. The partial derivatives of group velocity with respect to P wave velocity, shear velocity and density for the fundamental Rayleigh wave mode are plotted in Figure 11a, b, and c. The partial derivatives of group velocity with respect to shear velocity and density are plotted in Figure 12a, b for the fundamental Love wave mode. Figures 11 and 12 show a number of important factors that affect this study:

(1) The partial derivatives for P wave velocity in the upper crust are not insignificant when compared to density and shear velocity and therefore, affect the inversion.

(2) The P wave partial derivatives in the lower crust and mantle are small, and are not significant in the inversion.

(3) The partial derivatives with respect to shear velocity are larger than those for density and P

TABLE 6

STARTING MODEL
M2

LAYER THICKNESS	P-VELOCITY (KM/SEC)	SHEAR VELOCITY (KM/SEC)	DENSITY
5	5.5	3.0	2.8
5	5.5	3.0	2.8
5	5.5	3.1	3.05
5	5.5	3.1	3.05
10	6.0	3.5	3.1
10	6.0	3.5	3.1
10	8.1	4.6	3.3
10	8.1	4.6	3.3
10	8.0	4.4	3.3
15	8.0	4.4	3.3
25	8.0	4.4	3.37
25	8.0	4.4	3.37

RAYLEIGH WAVE

$\frac{DU}{DA}$

T, sec

FIGURE 11a

33

RAYLEIGH WAVE

T , sec

FIGURE 11b

$\frac{DU}{DB}$

34

RAYLEIGH WAVE

$\dfrac{DU}{D\rho}$

T , sec

FIGURE 11c

35

LOVE WAVE

$\dfrac{DU}{DB}$

T , sec

FIGURE 12a

36

LOVE WAVE

$\dfrac{DU}{D\rho}$

T, sec

FIGURE 12b

37
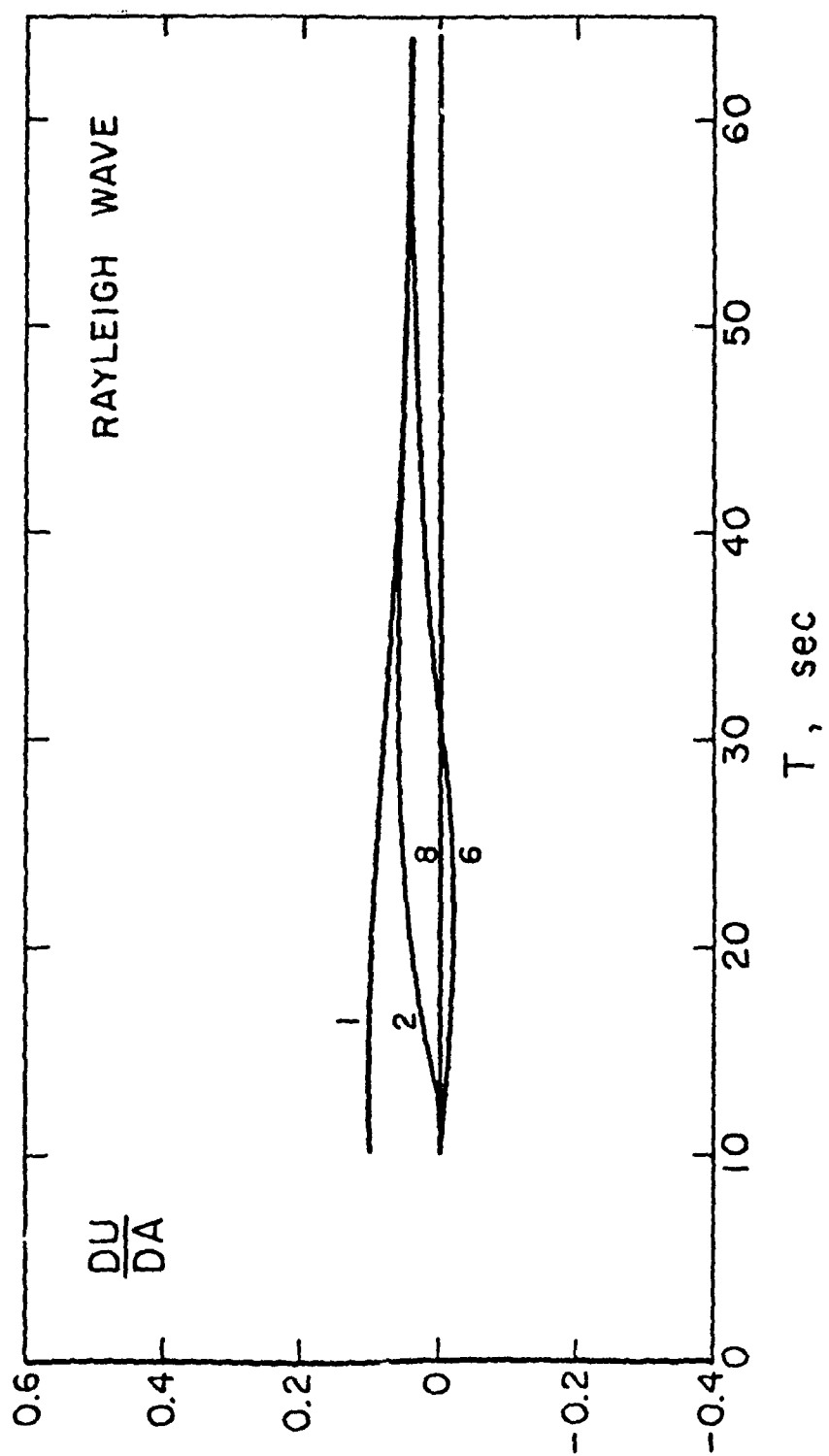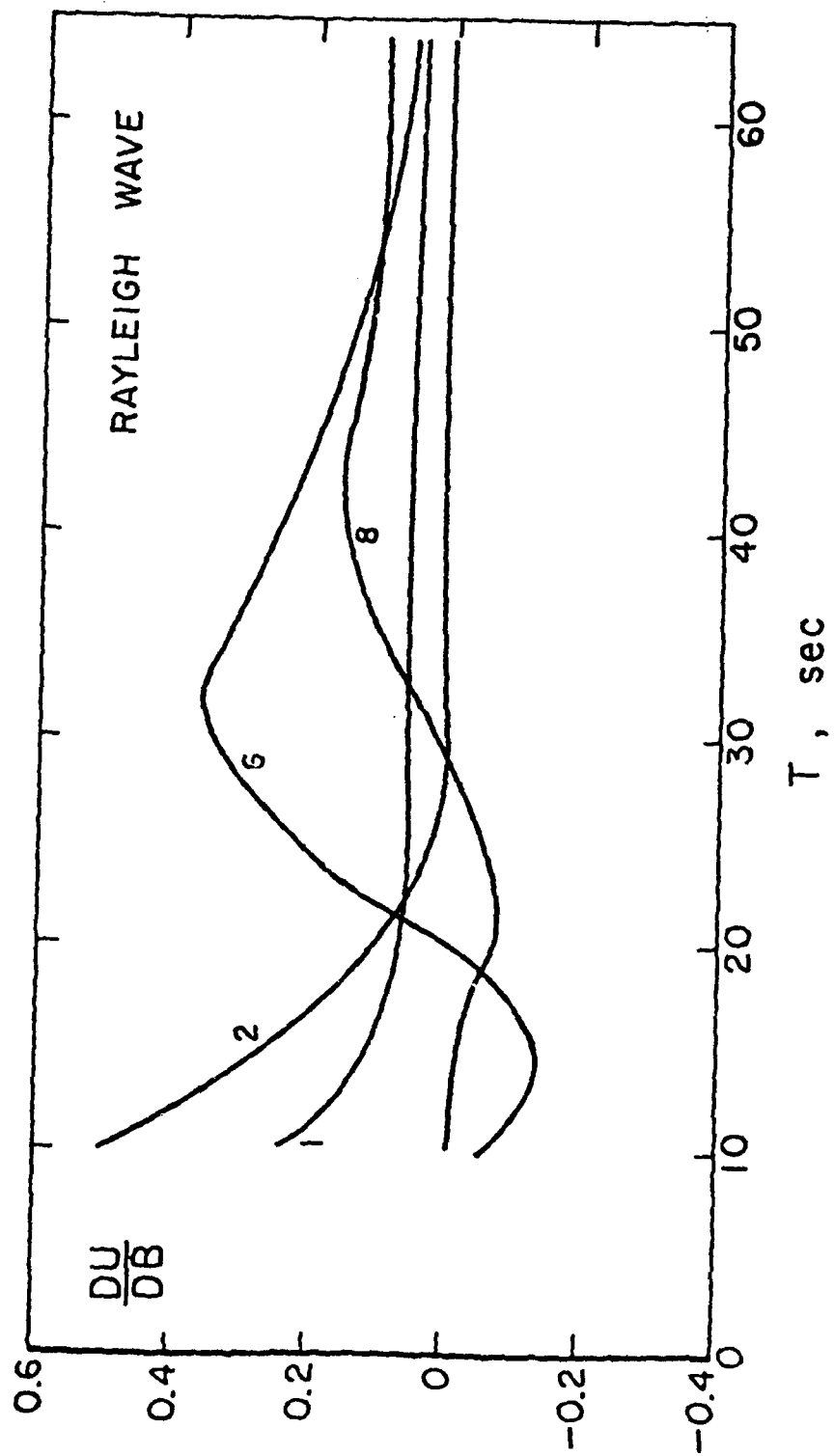
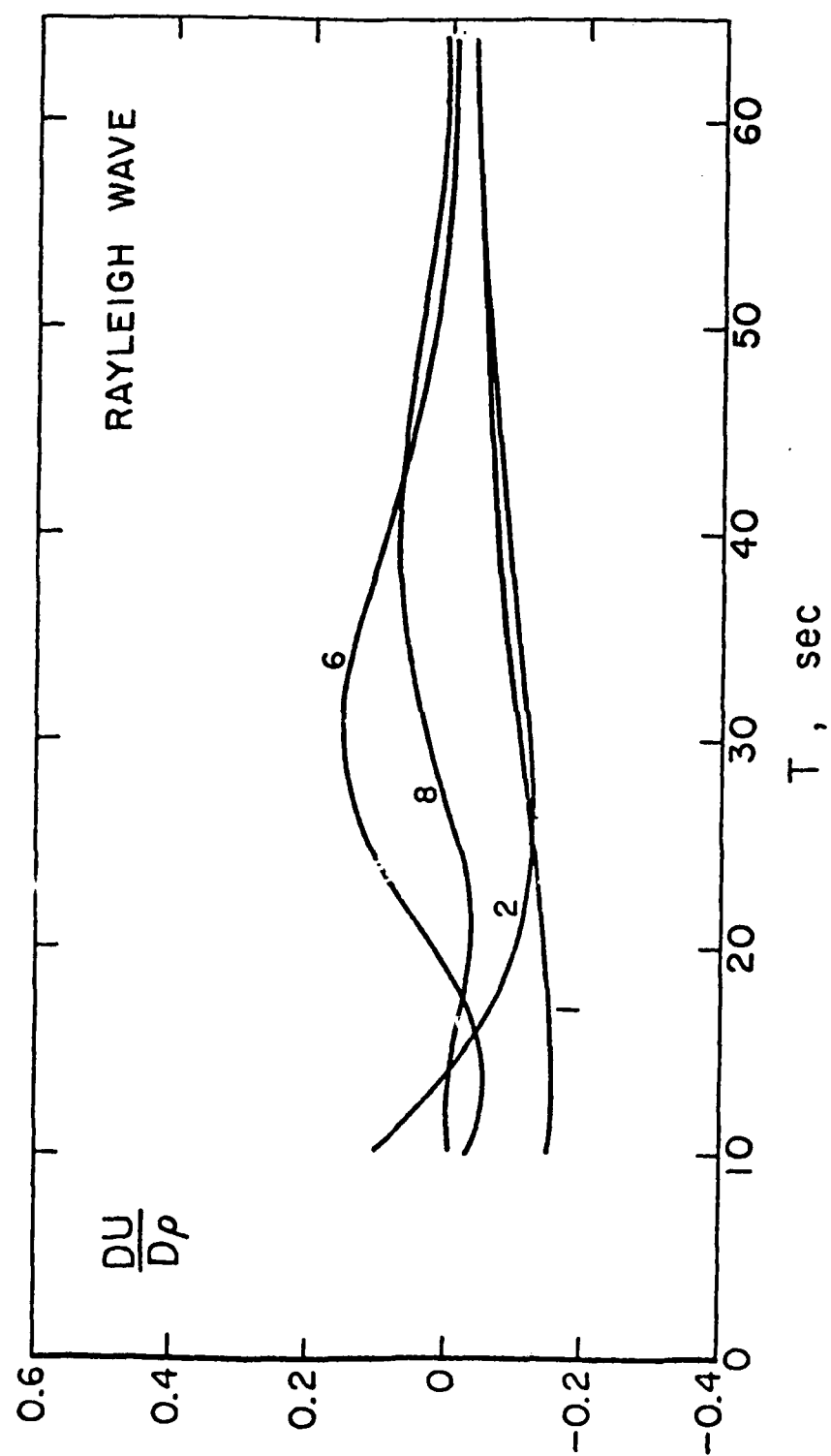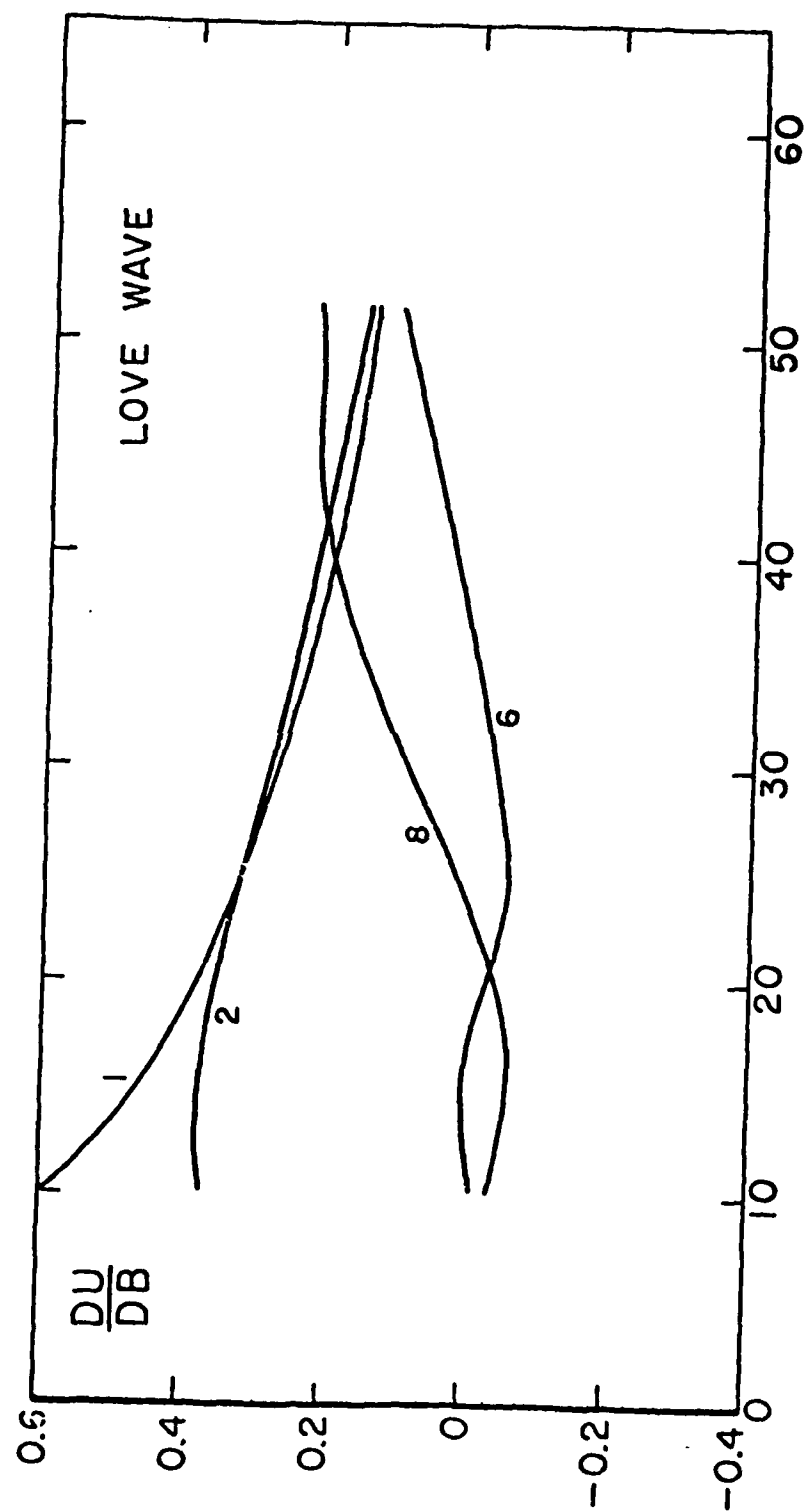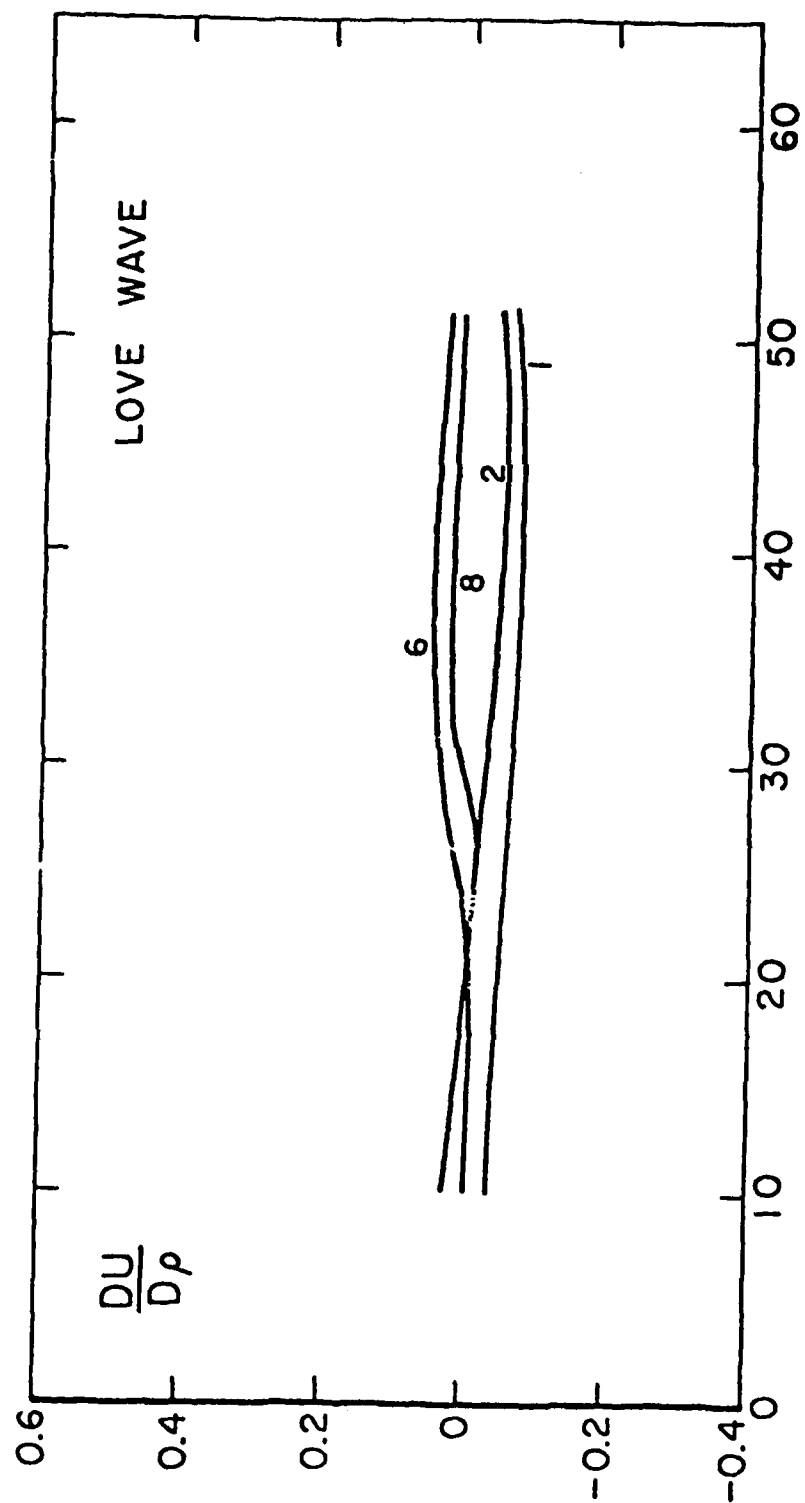wave velocity. Therefore, the resolution for shear
velocities is better than for the two other
parameters.

The starting model M2 and the derived model (SCS1)
with standard deviation error bars are shown in Figure 13.
The fit of theoretical group velocities for SCS1 are
shown in Figures 14 and 15. The averaging kernals are
listed in Table 7, where only the elements of the kernals
corresponding to the shear parameters are included. The
other elements for P wave velocity and density are small
and do not affect the structure. The width of these
kernals indicate that it is possible to resolve layers
to a thickness of 5 km in the upper crust, 10 km in the
middle crust and 20 km in the lower crust. However,
resolution in the mantle is quite poor. All the standard
deviations were found to be less than .08 km/sec.
Increasing the resolution in the lower crust and mantle
(by using a different trade-off parameter σ) leads to
instability in the shear velocity model, and unacceptably
large standard deviations. These features could be
improved if higher mode data were available.

The results of the inversion indicate that only a
few layers are justified to describe the crust with the
given dispersion information. As an option in the inver-
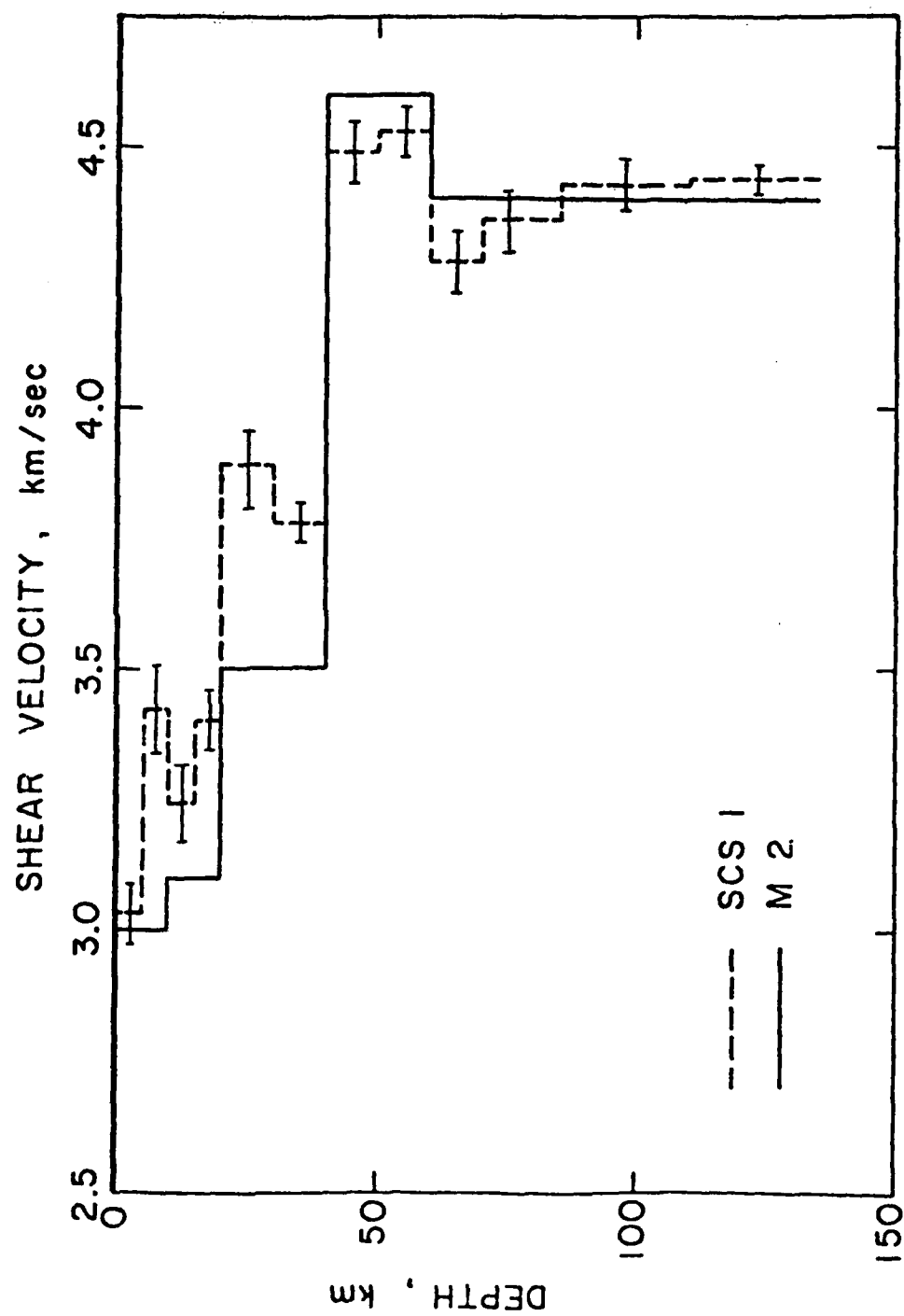sion program, averaging kernals can be made to resemble
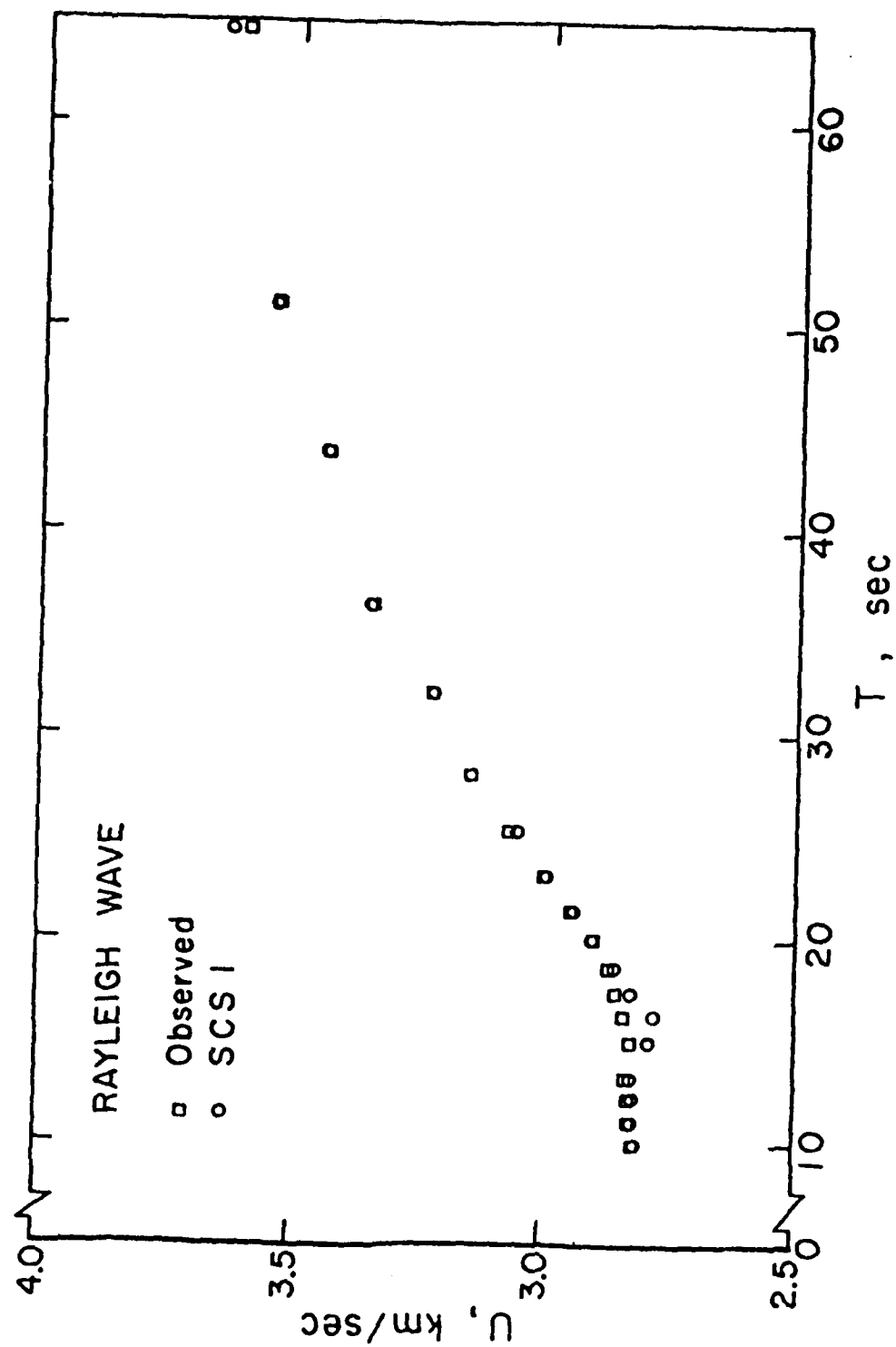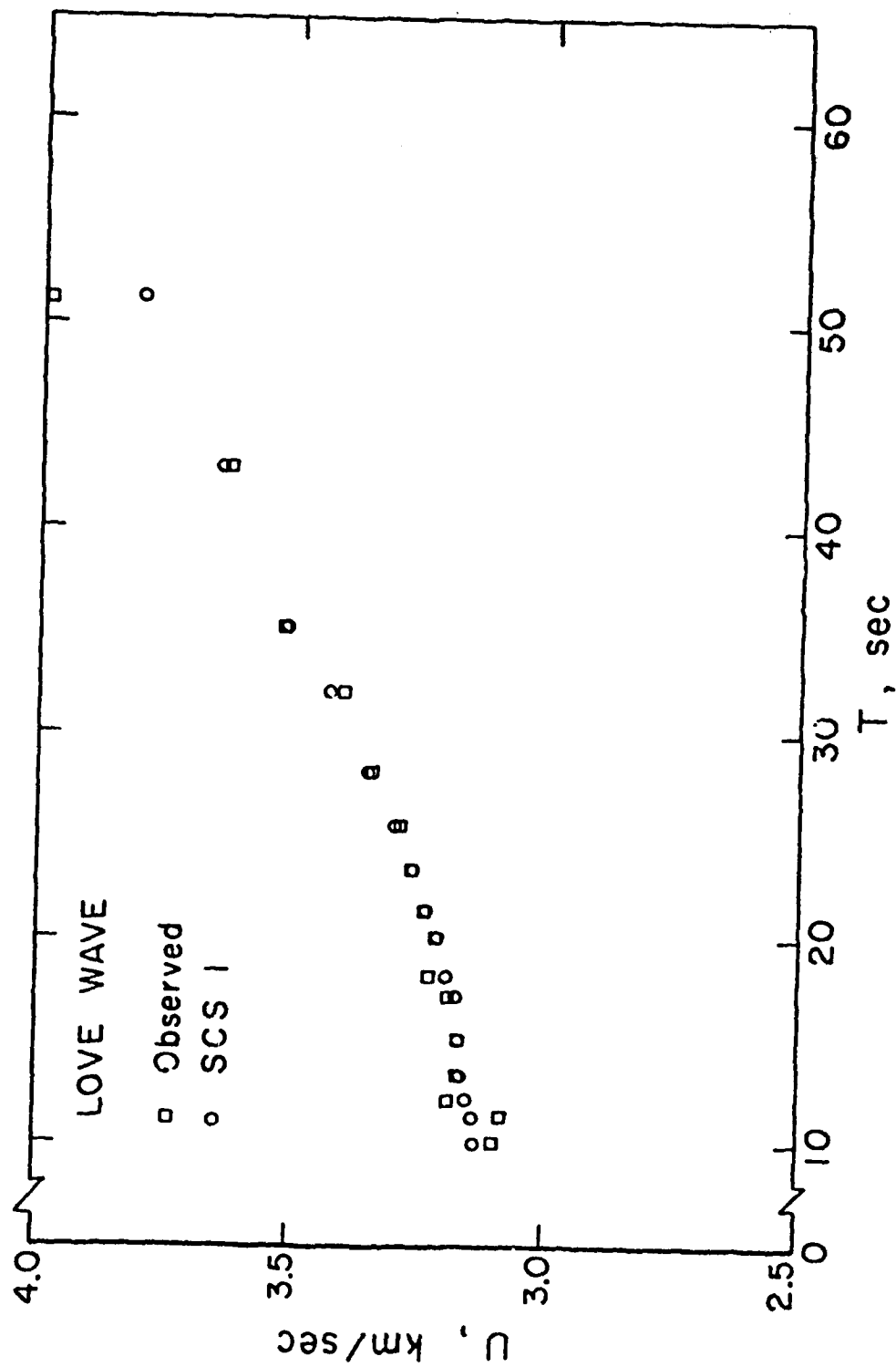
FIGURE 13

39

RAYLEIGH WAVE

□ Observed
○ SCS I

U, km/sec

T , sec

FIGURE 14

40

FIGURE 15

41

TABLE 7

RESOLVING MATRIX OF SHEAR PARAMETER

1.	.937	.096	-.058	.051	-.015	.008	-.002	.002	-.002	.001	.002	.002
2.	.096	.762	.259	.150	-.004	.030	-.004	-.014	-.006	-.002	-.003	-.003
3.	-.058	.260	.554	.316	-.016	-.065	.012	.026	.013	-.004	-.011	-.007
4.	.051	-.150	.317	.543	.184	-.056	-.051	-.009	.009	.008	-.002	-.004
5.	-.030	-.007	-.033	.368	.627	.281	-.017	-.087	-.054	-.019	-.001	-.009
6.	.015	.059	-.231	-.111	-.281	.526	.248	.080	-.081	-.074	-.055	-.024
7.	-.005	-.007	-.040	-.101	-.017	.248	.315	.222	.103	-.003	-.055	.043
8.	.0042	-.028	.051	-.019	-.087	.080	.222	.281	.229	.092	-.030	-.057
9.	-.005	-.011	.027	.018	-.054	-.031	.103	.229	-.244	.168	.023	-.047
10.	.010	-.013	-.057	-.006	.003	-.137	-.137	-.076	.058	.170	.160	.055

a desired box car vector. An example would be if we
wished to average the first two parameters, then we would
want the kernal to resemble a box car function such as
described in Table 8a. In the inversion, shear wave
parameters from layers 2, 3 and 4 were averaged, as were
parameters from layers 5 and 6, and layers 7 and 8,
Table 8c. The actual kernals for these averaged para-
meters are shown in Table 8b. The averaged values and
standard deviations are plotted in Figure 16. (Model
ASCS1, Table 9). A comparison with Tung and Teng (1974)
results indicates here that crustal shear velocities
are higher than previously reported values. And the lid
velocity in the mantle is found to be slightly less than
previously determined. A LVL at 60 km is consistent with
our dispersion data.

A list of the apriori and postpriori standard
deviations for SCS1 is given in Table 10. There is almost
no new information that can be derived from the data past
70 km. In the mantle in general, the amount of new
information from the data is quite small. But the
persistence of the LVL at the 60-70 km depth might indicate
a true velocity reversal and possibly the transition
between the lithosphere and asthenosphere.

43

TABLE 3

BOXCAR KERNAL FOR PARAMETERS 8a
1 and 2

1	1	0	0	0	0	0	0	0
1	0	0	0	0	0	0		
0	0	0						

ACTUAL BOXCAR AVERAGING KERNALS 8b

.089	.973	1.13	.710	.164	-.09	-.034	.002	.017	.002	-.015	-.015
-.015	.052	-.163	.256	.91	.81	.231	-.007	-.085	-.087	-.56	-.033
-.001	-.035	.091	-.12	-.10	3.27	.54	.502	.332	.097	.055	.099

THEORETICAL BOXCAR AVERAGING KERNALS 8c

1	1	1	0	0	0	0	0	0	0
0	0	0	1	1	0	0	0	0	0
0	0	0	0	0	1	1	0	0	0

FIGURE 16

45
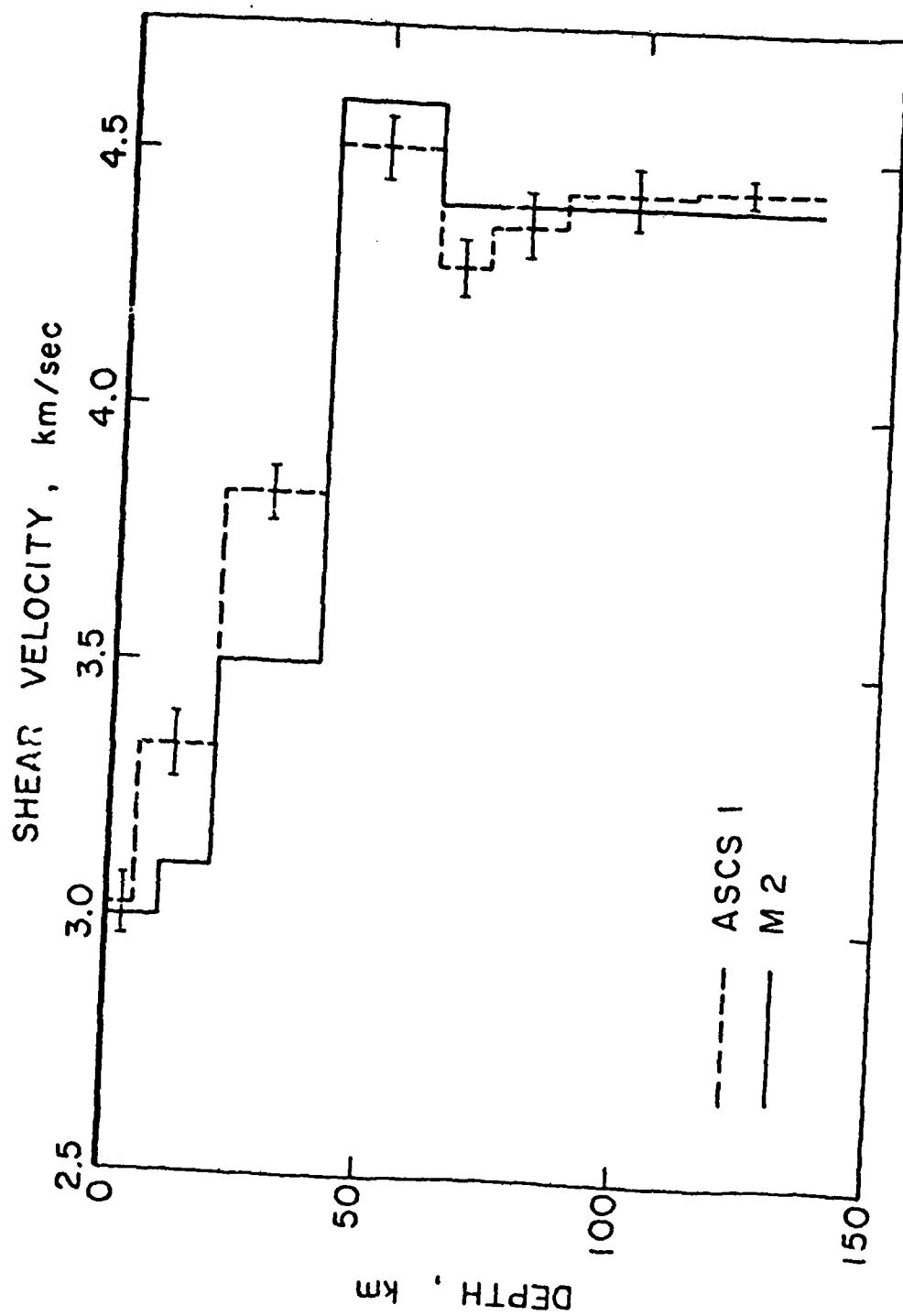
TABLE 9

MODEL ASCS 1

LAYER THICKNESS (KM)	SHEAR VELOCITY (KM/SEC)	SDX_0	SDX
5	3.03	.347	.087
15	3.36	.200	.062
20	3.84	.173	.065
20	4.51	.173	.120
10	4.28	.245	.210
15	4.36	.200	.175
25	4.44	.155	.142
25	4.44	.155	.150

TABLE 10

FINAL MODEL
SCP1

SHEAR VELOCITY	SDX_0	SDX
3.03	.347	.087
3.43	.347	.169
3.24	.347	.231
3.4	.347	.234
3.89	.245	.150
3.78	.245	.169
4.49	.245	.203
4.53	.245	.210
4.28	.200	.175
4.36	.155	.142
4.35	.155	.150

47

CONCLUSIONS

By comparing the size of the P-wave partial derivatives with density and shear wave partial derivatives, it was determined that compressional wave velocity cannot be neglected when inverting surface wave data. The resolution for shear velocity is better than the resolution for density and p-wave velocity.

The inversion of multi-layer models indicates that a 3 layer, 40 km crust adequately describes the South-China subplate. The resolution ranged from 5 to 20 km in the crust with model standard deviations of less than .08 km/sec. The shear velocities were found to be higher than those velocities reported by Tung (1974).

Upper mantle shear velocities were found to be lower than previously reported values. Resolution in the mantle was quite poor as no dispersion information is obtained from this study beyond 65 seconds. The apriori and postpriori standard deviation indicated that very little new information was being obtained from the data about the mantle. But because of the persistence of a LVL between 60 and 70 km, it is presumed that transition between the lithosphere and asthenosphere occurs here.

48

REFERENCES

REFERENCES

Backus, G. and Gilbert, F. (1967). Numerical Application
of a Formalism for Geophysical Inverse Problems:
Geophys. J. 13, p. 247-276.

Backus, G. and Gilbert, F. (1968). The Resolving Power of
Gross Earth Data: Geophys. J. 16, p. 169-205.

Braile, L. W. and Keller G. R. (1975). Fine Structure
of the Crust Inferred from Linear Inversion of
Rayleigh Wave Dispersion: Bull. Seism. Soc. Am.,
65, p. 71-82.

Crossen, R. S. (1976). Crustal Structure Modeling of
Earthquake Data 1, Simultaneous Least Squares
Estimation of Hypocenter: J. Geophys. Res., 81,
p. 3030-3046.

Der, Z. Masse, R. and Landisman, M. (1970). Effects of
Observational Errors on the Resolution of Surface
Waves at Intermediate Distances: J. Geophys. Res.
75, p. 3399-3409.

Der, Z., and Landisman, M. (1972). Theory for Errors,
Resolution, and Separation of Unknown Variables in
Inverse Problems, with Application to the Mantle and
Crust in Southern Africa and Scandinavia: Geophys.
J., 27, p. 137-179.

Dziewonski, A. and Hales, A. L. (1972). Numerical
    Analysis of Dispersed Seismic Waves: Method in
    Computational Physics, v. II, Academic Press, p. 306.

Dziewonski, A., Bloch, S., and Landisman, M. (1969).
    Technique for the Analysis of Transient Seismic
    Signals: Bull. Seism. Soc. Am., 59, p. 427-444.

Franklin, J. N. (1970). Well-Posed Stochastic Extensions
    of Ill-Posed Linear Problems: J. Math. Anal., 31,
    p. 682-716.

Hanson, R. J., and Lawson, C. L. (1973). Solving Least
    Squares Problems, Prentice Hall, Englewood Cliffs,
    N. J., p. 18-23.

Hermann, R. B. (1973). Some Aspects of Band-Pass Filtering
    of Surface Waves: Bull. Seism. Soc. Am., 63,
    p. 663-671.

Jackson, D. D. (1972). Interpretation of Inaccurate,
    Insufficient, and Inconsistent Data: Geophys. J.
    Roy. Astron. Soc., 28, p. 97-109.

Jordan, T. H., and Franklin, J. N. (1971). Optimal
    Solutions to a Linear Inverse Problem in Geophysics:
    Proc. Nat. Acad. Sci. U.S., 68, p. 291-293.

Kuichow Geologic Team 108 (1975). Features of Bedded
    Ultrabasic Rocks in Fairhinshun Region of Kuichow
    Province and a Preliminary Disucssion of their
    Origin: Scientia Geologica Sinica, 4, p. 343-351.

Li, C. Y. Cai, W. B., Ding, M. L., Xu, I. M., and Wang,
     Y. P. (1974). A Note on the Seismo-Geologic Features
     in China: Scientia Geologica Sinica, 1, p. 357-370.

Lee, W. H., Wu, F. T. and Jacobsen, C. (1976). A Catalog
     of Historical Earthquakes in China Compiled from
     Recent Chinese Publications: Bull. Seism. Soc.
     Am., 66, p. 2003-2016.

Sun, N. C. and Teng, T. (1977). Tectonic Plates of
     China: University of Southern California,
     Geophysical Laboratory Technical Report, 77-4.

Sung, C. H., Ho, G. T. and Hsu, G. M. (1965). A Study
     of the Sedimentary Layers in China: Acta Geophysica
     Sinica, 14, p. 158-167.

Tseng, J. S. and Sung, Z. A. (1963). Phase Velocity of
     Rayleigh Waves in China: Acta Geophysica Sinica,
     12, no. 2, p. 148-165.

Tung, J. P. (1974). The Surface Wave Study of Crustal
     and Upper Mantle Structure of Mainland China: Ph.D.
     dissertation, University of Southern California,
     248 p.

Wiggins, R. A., (1972). The General Linear Inverse
     Problems: Implications of Surface Waves and Free
     Oscillations for Earth Structure: Rev. Geophys.
     Space Phys., 10, p. 251-285.